The Journal of Chemical Physics

RESEARCH ARTICLE | FEBRUARY 03 2025

Superoxide anion (O_2^-) collisions with CO_2 molecules in the energy range of 50–950 eV

C. Guerra; M. Leiferman ; A. I. Lozano ; F. Aguilar-Galindo ; S. Díaz-Tendero ; J. C. Oller ; P. Limão-Vieira ; G. García

J. Chem. Phys. 162, 054303 (2025)
https://doi.org/10.1063/5.0242954

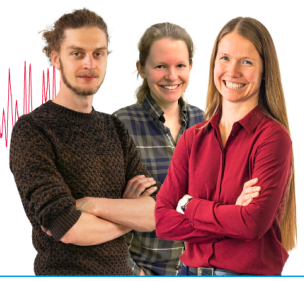

The Journal of Chemical Physics ARTICLE pubs.aip.org/aip/jcp

Superoxide anion (O_2^-) collisions with CO_2 molecules in the energy range of 50–950 eV

Cite as: J. Chem. Phys. 162, 054303 (2025); doi: 10.1063/5.0242954
Submitted: 8 October 2024 • Accepted: 9 January 2025 •
Published Online: 3 February 2025

C. Guerra,[1] M. Leiferman,[2] A. I. Lozano,[1,3,4] F. Aguilar-Galindo,[2,5] S. Díaz-Tendero,[2,5,6,a)] J. C. Oller,[7] P. Limão-Vieira,[3] and G. García[1,8,a)]

AFFILIATIONS

[1] Instituto de Física Fundamental, Consejo Superior de Investigaciones Científicas, Serrano 113-bis, 28006 Madrid, Spain
[2] Departamento de Química, Módulo 13, Universidad Autónoma de Madrid, 28049 Madrid, Spain
[3] Laboratório de Colisões Atómicas e Moleculares, CEFITEC, Departamento de Física, Universidade NOVA de Lisboa, 2829-516 Caparica, Portugal
[4] Institut de Recherche en Astrophysique et Planétologie (IRAP), Université Toulouse III -Paul Sabatier, 9 Avenue du Colonel Roche, Toulouse 31028, France
[5] Institute for Advanced Research in Chemistry (IAdChem), Universidad Autónoma de Madrid, 28049 Madrid, Spain
[6] Condensed Matter Physics Center (IFIMAC), Universidad Autónoma de Madrid, 28049 Madrid, Spain
[7] División de Tecnología e Investigación Científica, Centro de Investigaciones Energéticas, Medioambientales y Tecnológicas, 28040 Madrid, Spain
[8] Centre for Medical Radiation Physics, University of Wollongong, NSW 2522, Australia

[a)] **Authors to whom correspondence should be addressed:** sergio.diaztendero@uam.es and g.garcia@csic.es

ABSTRACT

A novel gas-phase molecular scattering study is reported for O_2^- collisions with CO_2 for impact energies ranging from 50 to 950 eV in the lab frame. The absolute total electron detachment, relative total, and partial ionization cross sections have been measured within this energy range together with the positive ion yields. The primary anionic beam projectile is produced in a pulsed hollow cathode discharge induced plasma, and its interactions with the neutral molecular target occur in a gas cell at a well-known constant pressure. For impact energies above 500 eV, high mass (m > 44 u) charged complexes have been detected. With the aid of a theoretical study using *ab initio* methods, we propose a mechanism to infer the formation of these cationic species, which have been assigned to projectile–target stable compounds (CO_3^+ and CO_4^+).

I. INTRODUCTION

The CO_2 molecule has acquired an increasing interest in recent decades due to its relevance in laser technology[1] with significant applications in medicine.[2] It plays an important role in plasma diagnostics,[3,4] solving atmospheric[5] and astrophysical issues,[6] as well as modeling particle transport in gas mixtures.[7] The atmospheric concentration of CO_2 affects basically plant metabolism,[8,9] global warming,[10,11] and other environmental parameters directly related to the stability of the biosphere.[12]

CO_2 electronic structure and dissociation patterns have been studied through photoabsorption experiments.[13–15] Electron and positron scattering by CO_2 have also been the subject of many theoretical and experimental studies, and the interaction cross section data have been recently summarized.[16]

Negative ions (H^-, D^-, He^-, F^-, Cl^-, I^-, NO^-, and O^-) colliding with CO_2 have been studied by different authors, paying special attention to electron detachment, charge exchange, and resonant processes.[17–21] Paulson[22] conducted a comprehensive study on the reactions $O^- + CO_2 \rightarrow CO_2^- + O$, $O^- + CO_2 \rightarrow O_2^- + CO$, $NO^- + CO_2 \rightarrow CO_2^- + NO$, $O_2^- + CO_2 \rightarrow CO_3^- + O$, and $O_2^- + CO_2 \rightarrow CO_2^- + O_2$, thus obtaining effective cross section values for energy ranges between 1 and 100 eV. Negative ion reactions with different molecular targets, including CO_2, were also reported by

Moruzzi and Phelps.[23] Doverspike *et al.*[24] reported absolute electron detachment cross sections for colliding anionic projectiles (Cl^- and Br^-) with different neutral molecular targets H_2, D_2, O_2, N_2, CO, CO_2, and CH_4, in the energy range between 1 and 300 eV.

As far as cation collisions with CO_2 studies are concerned, we note extensive discussion in the literature. Greenwood *et al.*[25] implemented a novel experimental beam line to study a certain type of collision that occurs in the interaction of solar wind ions with cometary gases, obtaining absolute measurements of the charge-exchange cross sections for collisions of highly charged ions (H^+, He^+, and He^{2+}) with neutral targets (H_2O and CO_2) in the impact energy range of 0.3–7.5 keV.

The superoxide anion (O_2^-) is one of the reactive oxygen species (ROS) whose significance in diverse chemical and biological systems attracted the interest of many investigations.[26] Due to its reactive properties, it plays an important role in biomedical[27,28] and industrial[29] applications. The chemistry of O_2^- in space has also been recently analyzed.[30] However, superoxide anion scattering cross section data for relevant biological and environmental molecules are scarce. In particular, as far as we know, apart from the aforementioned anion reaction studies,[22] collisional data of O_2^- with CO_2 are not reported in the literature.

In this study, we present a theoretical and experimental investigation of collisions of O_2^- with CO_2 in the gas-phase. Absolute total electron detachment cross sections (TEDCSs) for impact energies ranging from 50 to 950 eV have been measured with a transmission-beam experimental system.[31] We have also obtained relative total ionization cross sections (TICSs) by analyzing the ion formation intensities with respect to that of the primary ion beam for each incident anion energy. The induced cationic fragmentation has been calculated by means of quantum chemistry simulations, proposing the mechanism for the formation of stable CO_3^+ and CO_4^+ compounds.

The remainder of the present paper is organized as follows. In Sec. II, we describe the experimental procedure and analyze the possible uncertainty sources. The theoretical methods are described in Sec. III. In Sec. IV, we present and discuss the obtained results. Finally, in Sec. V, we summarize the main conclusions of this study.

II. EXPERIMENTAL PROCEDURE

A. Apparatus

The experimental system has been entirely described in previous publications,[31–34] and therefore, we will only briefly present here some operational details.

The incident anion beam is generated in a hollow-cathode plasma discharge produced by a pulsed oxygen molecular beam from a supersonic expansion and passes through a 20 mm length cylinder negatively biased (around −500 V). Negative ions, produced in the discharge afterglow, are then accelerated by the cathode voltage and focused on the scattering chamber entrance aperture (2 mm in diameter). As shown in Fig. 1 of Ref. 33, a parallel electrostatic plate system controls the direction of the beam, and a perpendicular magnetic field produced by external magnets removes the electrons and contributes to separate in mass the components of the anion beam. The scattering chamber is a gas cell (GC) where the molecular target is introduced at well-known pressures that were varied from 0 to 2 mTorr according to the measurement requirements.[31]

The anionic oxygen beam is accelerated or decelerated by applying a negative or positive voltage to GC, thus defining the kinetic energy of the O_2^- anions during the collision. The positive ions produced by O_2^-–CO_2 interactions in the GC are extracted and accelerated, by means of an extractive plate system, through a time-of-flight (TOF) mass spectrometer (1.40 m length) normal to the plane of collision. The ions produced are finally detected by a microchannel plate detector (MCP1) operating in single pulse counting mode to facilitate their mass analysis. The extraction parallel plates are connected to positive (0 to +900) and negative (0 to −900) pulsed voltages, respectively. The voltage and duration of these pulses were optimized to ensure a total and uniform ion extraction while maintaining a reasonable mass resolution. Typical values in this case were +350 and −50 V, respectively, for the extractive pulses with a duration pulse of about 4 μs. The length of the hollow cathode limits the mass resolution (see Ref. 31), which is about $\Delta m/m = 0.05$.

The experimental setup also incorporates a homemade electron gun placed under the GC that provides an energy-controlled electron beam of 0–500 eV kinetic energy crossing the interaction region perpendicularly to the anion beam and opposite to the TOF mass analyzer. The main purpose of the electron gun is to analyze the molecular composition of the background and provide the electron induced ionization patterns as a function of the incident electron energy, which will be useful to compare to those induced by the anion beam.

Finally, the transmitted anionic beam is perpendicularly repelled by a continuous −250V voltage toward a second microchannel plate detector (MCP2), which monitors the primary anion beam intensity. The MCP2 detector signal is also used to determine the primary beam energy distribution by using a set of three grids as a retarding field analyzer placed at the entrance of the transmission chamber (see Refs. 31–34 for details).

The projectile anionic beam is mainly formed by O_2^-, but, despite the filter mentioned above, it also contains certain traces of O^- and O_3^-. A typical TOF mass spectrum of the primary beam of 470 eV kinetic energy is plotted in Fig. 1. The main contribution to the beam intensity is due to O_2^-, and the relative delay between the O^-–O_2^- beams is 17 μs, while for the O_2^-–O_3^- it is about 15 μs. Tuning the extraction pulses, we can select the area of the primary beam that is really generating the positive ion fragments being mass analyzed (see Fig. 1). This procedure acts as a TOF filter of the primary anion beam and guarantees no contamination from the O^- and O_3^- components of the anion beam. Note that the area corresponding to the fraction of the anion beam (the area above the dashed red line in Fig. 1) that is producing the extracted cations is 100% formed by O_2^-.

B. Data acquisition methodology

1. Measurement methodology

The TEDCS (σ_t) for O_2^- collisions with CO_2, within the impact energy range of 50–950 eV, has been obtained by measuring the primary anion beam attenuation as a function of the target (CO_2) pressure from 0 to 2 mTorr. Details on the absolute gas pressure measurements, the transmitted O_2^- detection, and the procedure to derive the TCS values from the attenuation curves can be found in Refs. 31–34. Figure 2 shows some typical attenuation curves for different impact energies ranging from 50 to 900 eV.

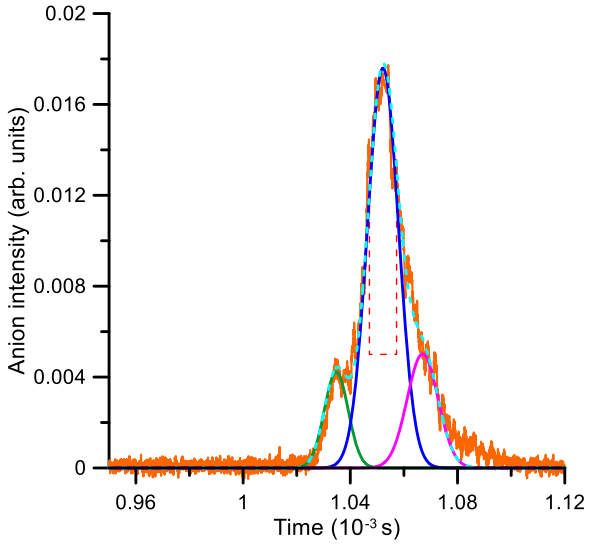

FIG. 1. Time of flight mass spectrum of the primary anion beam for 470 eV incident energy. Orange solid line: experimental TOF spectrum; and sky blue dashed line: Gaussian fit for the three components of the primary beam: green solid line: O^-, blue solid line: O_2^-, and pink solid line: O_3^-. Red dashed line: line delimiting the area corresponding to the fraction of the primary beam that is producing the extracted cations.

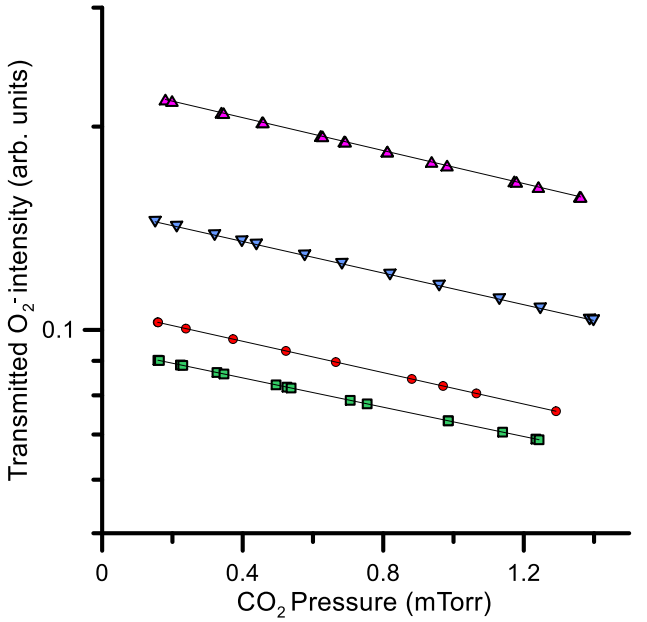

FIG. 2. Transmitted O_2^- intensity as a function of the CO_2 pressure in the gas cell for 50 (red filled circle), 250 (green filled square), 500 (pink filled triangle), and 900 (blue filled triangle) eV impact energies. Semilogarithmic fits of the experimental data are also plotted (black solid line).

On the other hand, the TICS (σ_+) is derived from the ratio between the total positive ion detected intensity and the primary anion intensity. Details on anion and cation current detection and the limitation to obtain absolute values from the present measurements are discussed in Ref. 33.

2. Uncertainty analysis

Concerning the TEDCS, statistical uncertainties have been constrained below 5% by repeating at least five times the anion attenuation measurements and their corresponding data acquisition and analysis procedures for each impact energy considered in this study. Since the attenuation, as a function of pressure, is determined at the peak of the transmitted TOF mass spectrum, Fig. 1 shows that only the O_2^- intensity contributes to the measurements. We then consider that the present results are discriminated from possible O^- and O_3^- contributions. The accuracy of the pressure determination is given by the uncertainty limit of the absolute capacitance manometer used (1%, according to the manufacturer data). However, due to pressure gradients in the gas cell, we considered the gas pressure as the average of those measured at both sides of the cell, thus introducing an additional error contribution to the experimental cross sections of about 7%. Adding *in quadrature* all the known error sources and statistical uncertainties, we determine a total uncertainty limit of 8%–10% for the absolute electron detachment cross sections. With respect to the relative ionization cross section, instabilities in the hollow cathode discharge led to statistical uncertainties of 7%–14%, depending on the impact energy. Combining all the above error sources, the total uncertainty limit for these measurements has been determined to be within 10%–16%. The influence of external fields or secondary effects in the present measurements has been minimized by guiding the primary and secondary beams with electrostatic plate systems and optimizing the voltage duration and synchronism of the extraction pulse. We consider the present data as the result of single anion–molecule collisions only, without impacts from the environment.

III. COMPUTATIONAL DETAILS

We have thoroughly explored the potential energy surfaces of the neutral, anionic, and cationic species involved in the collision, including different spin multiplicities. The geometry optimizations were performed using the Møller–Plesset perturbation theory, a post-Hartree–Fock *ab initio* method, including perturbations up to second order (MP2)[35] in combination with the aug-cc-pVTZ basis set.[36] We further computed the harmonic frequencies over the optimized geometries at the same level of theory to verify that they are minima in the corresponding potential energy surface and to obtain thermochemical values.[37] More accurate relative energies for each considered species were obtained by means of coupled cluster calculations,[38] including single and double excitations and the triplet ones perturbatively, CCSD(T), with the same basis set aug-cc-pVTZ, also over the geometry previously optimized. All these calculations were performed with the Gaussian16 program.[39]

IV. RESULTS AND DISCUSSIONS

A. Induced fragmentation

Figure 3 shows the TOF mass spectrum for the cation fragmentation induced by collisions of O_2^- with CO_2 at the impact energy of 650 eV. The assignments are tabulated in Table I. The CO_2 cationic fragmentation has been analyzed for impact energies ranging from

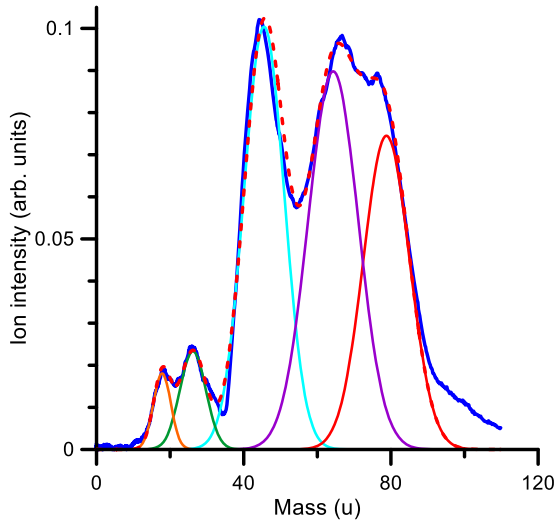

FIG. 3. TOF mass spectrum of the positive ion induced fragmentation of CO_2 in collisions with 650 eV oxygen anions (O_2^-). Gaussian fitting analysis: *m/z(u)* = 16/17 (orange solid line), 27/28 (green solid line), 44 (sky blue solid line), 60–64 (pink solid line), and 73–77 (red solid line). (See also the proposed cation assignments shown in Table I.)

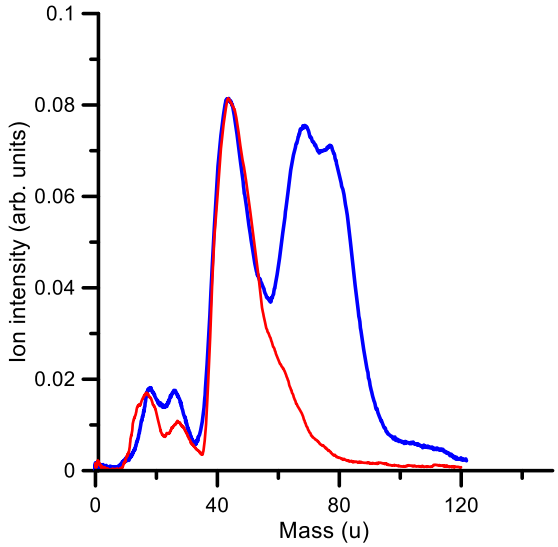

FIG. 4. Positive ion induced fragmentation by the superoxide anion beam (blue solid line) and the electron beam (red solid line), respectively, both at 600 eV impact energy.

150 to 900 eV by measuring the intensity of each TOF mass feature, corresponding to each identified fragment, with respect to that of the parent ion (m/z = 44 u).

A close analysis of Fig. 3 reveals the most intense cationic fragment can be assigned to the parent ion CO_2^+, and those fragments with 16/17 and 27/28 m/z can be related to O^+ and CO^+ fragments, respectively. Surprisingly, two structures with m/z greater than the parent ion (m/z at about 60–64 and 74–76) have also been observed in the mass spectra. These fragments have been tentatively assigned to the formation of $(CO_2{\cdot}O)^+$ and $(CO_2{\cdot}O_2)^+$ complexes. At this point, it is interesting to compare the fragmentation induced by the anion beam to that produced by the electron beam (described in Sec. II) in similar collision conditions. The results are shown in Fig. 4, where both spectra are normalized to the parent ion (m/z = 44) yield. As this figure shows, O_2^- projectiles produce a higher m/z fragmentation than electrons. The main difference corresponds to the formation of molecular compounds with masses higher than that of the parent ion ($m/z > 44$). Since the low-pressure conditions of this experiment ensure that only binary collisions may take place, such high mass compounds have to be formed by the capture of a projectile molecule by a target molecule. This is not attained when the projectile is an electron. The intensity enhancement of fragments with $m/z \cong 28$ suggests that these high-mass compounds may decay via CO^+ formation. Understanding the origin of these fragments ($m/z \geq 44$) represents a major challenge and requires a detailed theoretical analysis to recognize the possible reaction mechanisms underlying the rather complex collision dynamics (see Sec. IV B). Nevertheless, we have previously obtained similar results in our recent study on O_2^- collisions with benzene,[32] where the formation of large complex molecules has been reported. In such a joint experimental and theoretical study,[32] we proposed the formation of $C_6H_6O_2^+$ via a sudden double ionization of benzene and the subsequent electrostatic attraction between the O_2^- and the dication formed, thus leading to stable diol structures. This mechanism is consistent with further partial and total ionization cross section measurements as noted in Ref. 34.

TABLE I. TOF features formed in O_2^- collisions with CO_2 and tentative cationic species assignation.

Mass (m/z)	Proposed assignment
16/17	O^+
27/28	CO^+
44	CO_2^+
62–64	$(CO_2{\cdot}O)^+$
74–76	$(CO_2{\cdot}O_2)^+$

To analyze the variation of each fragment intensity as a function of the collision energy, Fig. 5 shows the relative intensity of the positive ion fragments produced by the collision of O_2^- with CO_2 for the whole impact energy range considered in this study (160–900 eV). For impact energies below 600 eV, the most intense fragment is found to be the parent ion, followed by those fragments with higher masses ($m/z > 44$). However, between 600 and 900 eV, the intensity of those fragments increases and is comparable to that of the parent ion. Therefore, we can expect that the major contribution to the total ionization cross section, in the investigated energy range, results from the formation of the parent ion (m/z = 44) and the high-mass compounds, especially in the 600–900 eV impact energy range.

B. Structures and mechanistic proposal

Figure 6 shows a mechanistic proposal of the relative energies for the formation of high mass cationic species. We present in the

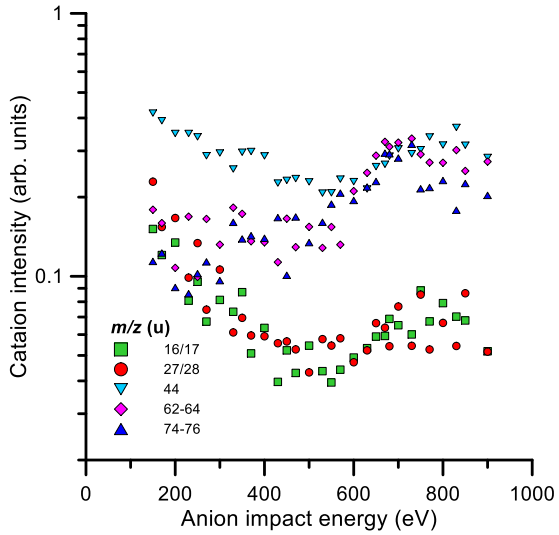

FIG. 5. Relative intensity of the different cation species detected by the TOF mass spectrometer: green filled square: O^+, red filled circle: CO^+, sky blue down-pointing triangle: CO_2^+, pink diamond: $(CO_2{\cdot}O)^+$, and blue up-pointing triangle: $(CO_2{\cdot}O_2)^+$.

figure relative enthalpies, ΔH, for different points in the potential energy surfaces, referred to as the entrance channel $CO_2 + O_2^-$. Detection of cationic species with high mass implies the ejection of two electrons accompanied by the reaction of the ionized formed species. Double ionization channels can be achieved by direct emission of two electrons or in a sequential two-step mechanism, i.e., single ionization in a high-energy state followed by autoionization leading to the doubly ionized channels. The highest energy channel that we have considered corresponds to a situation in which the two electrons are ejected from CO_2, and it is found at almost 40 eV with respect to the entrance channel. Charge exchange processes would lead to CO_2^+, detected in the experiment (m/z = 44). We also identify oxygen exchange channels, where CO^+ (m/z = 28) and CO_3^+ (m/z = 60) appear at ~19 and 21 eV, respectively. Finally, we also show the relative energy range in which the formation of the complex $[CO_2{\cdot}O_2]^+$ or CO_4^+ species takes place at ~12 to 19.5 eV. The corresponding computed structures are given in Fig. 7. Some of these correspond to compounds bonded through van der Waals forces; the rest show covalent bonds stabilizing a CO_4^+ structure. Both kinds of structures have been found in the potential energy surfaces with doublet and quartet spin multiplicity.

The experimental detection of CO^+, CO_3^+, and CO_4^+ implies a population of channels well above the ground state of the doubly ionized channels, $CO_2(^1\Pi_u) + O_2^+(^2\Pi_g)$. Therefore, the energy appearance of such species in the calculations indicates that highly charged CO_2^{2+} and/or highly energetic states of the $[CO_2{\cdot}O_2]^+$ complex are populated in the collision following double ionization. One possible path to form the experimentally detected complexes would imply the electrostatic attraction of CO_2^{2+} and O_2^- forming the $[CO_2{\cdot}O_2]^+$ complex. Another possible path could be the evolution of states with high internal energy into CO_4^+ stable structures. Notwithstanding, in both cases, CO_4^+ and CO_3^+ channels can be energetically achieved.

C. Total electron detachment and total ionization cross sections

The absolute total electron detachment cross section (TEDCS) in the energy range of 50–950 eV, together with the relative total ionization cross section (TICS) for energies ranging from 160 to 900 eV, obtained with the experimental procedures described above, are shown in Fig. 8. Numerical data are also presented in Tables II and III, respectively. A close inspection of this figure shows that the TEDCS slightly decreases in magnitude while energy increases up to 250 eV and, subsequently, increases up to 550 eV, reaching a plateau for higher energies. This behavior is consistent with previous results for collisions of different positive and negative ions with CO_2.[17,19,22,40] In addition, a feature like a shoulder between 300 and

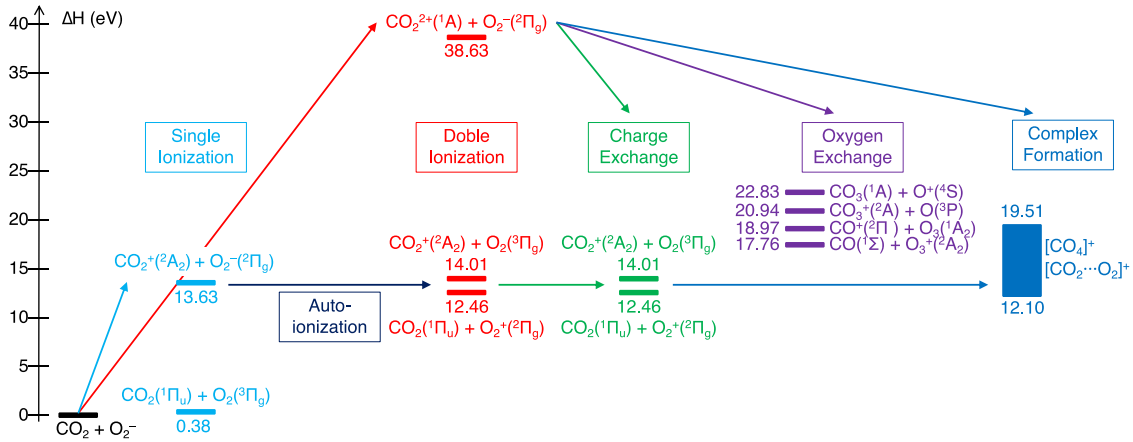

FIG. 6. Relative energies (enthalpy) of the different species involved in the mechanisms referred to the initial reactants in the collision $CO_2 + O_2^-$. Different colors denote different processes or final products.

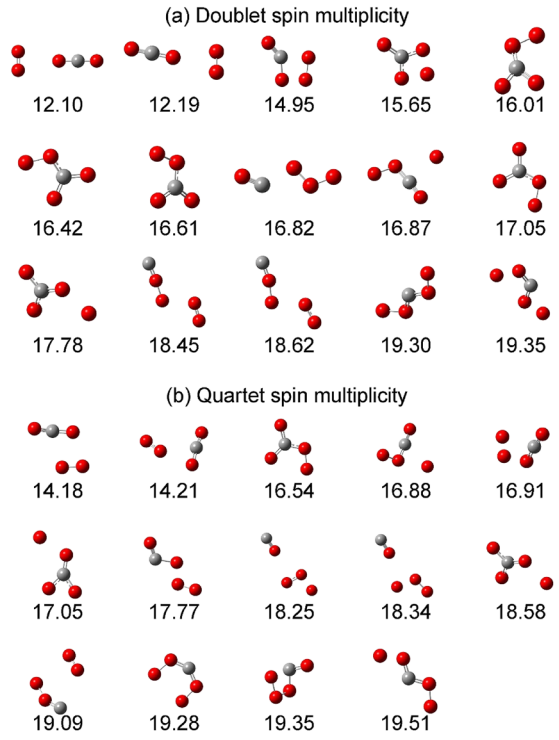

FIG. 7. Optimized structures of the exit channels for the $[CO_4]^+$ molecules (or $[CO_x{\cdot}O_{4-x}]^+$ complexes), with the two possible spin multiplicities: (a) doublet; (b) quartet. Numbers show the relative energy (enthalpy in eV) of the corresponding structure referred to the initial reactants in the collision $CO_2 + O_2^-$.

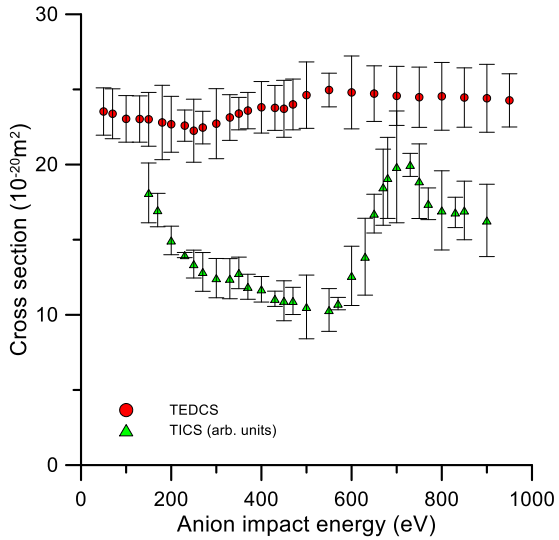

FIG. 8. TEDCS (red filled circle) in the 50–950 eV energy range for O_2^- collision with CO_2 and relative TICS (green filled triangle) for the impact energy range of 150 to 900 eV for the formation of positive ions. Note that the TICSs are just relative values in arbitrary units.

TABLE II. Present experimental results of the TEDCS for O_2^- anion collisions with CO_2 together with their associated uncertainties.

Energy (eV)	TEDCS ($\times 10^{-20}$ m^2)	Total uncertainty (±)
50	23.53	1.57
70	23.38	1.66
100	23.04	1.55
130	23.03	1.54
150	23.01	1.79
180	22.80	2.47
200	22.68	1.86
230	22.59	1.03
250	22.25	2.09
270	22.46	1.08
300	22.72	2.33
330	23.13	1.52
350	23.39	1.08
370	23.59	1.20
400	23.81	1.71
430	23.77	1.49
450	23.71	1.89
470	24.00	1.69
500	24.62	2.20
550	24.96	1.11
600	24.80	2.42
650	24.72	1.85
700	24.57	1.96
750	24.48	2.00
800	24.54	2.25
850	24.46	1.97
900	24.41	2.26
950	24.27	1.76

450 eV is noted, with a local maximum at around 400 eV. Although the origin of this feature is not clear, it could be in part associated with ionization processes as we will discuss below. Formation of resonances from charge exchange processes (see Refs. 20 and 21) has shown that such processes can occur at relatively high energies, at around 2 keV and 100 eV in the cases of CO_2 and O_2, respectively. Similarly, Huq[19] obtained results in full agreement with Tuan *et al.*,[20] the latter concluding that multiple resonances are present in the reaction $H^- + CO_2$, noting the remarkable and evident influence of $^2\Pi_u$ resonance states on electron detachment dynamics for collision energies above 100 eV. This would be reflected in the increase in the TEDCS that we observe in the present study, thus revealing that the direct detachment of electrons would be the predominant process at lower collision energies.

We have not found in the literature previous electron detachment cross section data for O_2^- collisions with CO_2 to compare with the present results. However, in comparison with our recent study with oxygen as a molecular target,[33] the corresponding TEDCS shows a similar trend, almost constant along the considered impact energy range, but the absolute values for CO_2 are about 70% higher in magnitude than those for O_2. This ratio is similar to that of their corresponding molecular polarizabilities (2.507 and 1.562 Å^3, respectively[40]), thus suggesting that this parameter probably plays

TABLE III. Present relative values of the total ionization cross section (TICS) for O_2^- anion collisions with CO_2, together with their associated uncertainties.

Energy (eV)	TICS (arb. Units)	Total uncertainty (±)
150	10.99	1.99
170	6.56	1.11
200	6.35	0.94
230	1.22	0.17
250	6.93	0.92
270	10.04	1.29
300	10.51	1.30
330	10.78	1.33
350	8.20	1.04
370	7.03	0.83
400	7.28	0.85
430	4.59	0.50
450	12.15	1.32
470	8.27	0.90
500	20.15	2.12
550	13.77	1.42
570	3.84	0.41
600	15.66	1.97
630	18.44	2.55
650	7.70	1.28
670	13.69	2.53
680	14.12	2.69
700	18.75	3.72
730	3.84	0.76
750	13.15	2.48
770	10.99	1.05
800	6.56	2.63
830	6.35	1.01
850	1.22	1.94
900	6.93	2.40

an important role in the electron detachment process. This result is consistent with our previous measurements on N_2 and recent studies on O_2 and N_2[41,42] using other anion projectiles such as O^-, CH^-, and CH_2^-.

In contrast, the results for the relative TICS from the measured positive ion yields (see Table II) show a different behavior. They sharply decrease for increasing energies up to 550 eV, then notably increase up to 700 eV and again decrease for higher energies. The TICS profile exhibits two local maxima at around 350 and 730 eV (see Fig. 5). From the local maximum found at 350 eV close to the shoulder in the TEDCS above 300 eV, we can consider both as being partially associated. Similar behavior has been noted in our previous study on O_2^- collisions with N_2.[31] The second local maximum in the TICS is found around 700 eV. Since we only obtained relative values, it is difficult to evaluate its correlation with the corresponding TEDCS. However, as derived from the partial ICS shown in Fig. 6, the main contributions to this maximum arise from the formation of higher mass complexes assigned to $(CO_2{\cdot}O)^+$ and $(CO_2{\cdot}O_2)^+$. This is consistent with a similar conclusion in the case of O_2^- collisions with benzene.[34]

V. CONCLUSIONS

We have measured for the first time absolute TEDCS for O_2^- collisions with CO_2 for impact energies ranging from 50 to 950 eV by using an anion beam transmission technique. Relative partial and total ionization cross sections in the energy range 150–900 eV have been obtained by analyzing the mass of the cations formed during the collision processes by means of a TOF mass spectrometer. For impact energies up to about 500 eV, the most intense cation signal corresponds to the parent ion (CO_2^+) formation. However, within the energy range of 500–900 eV, intense ion signals corresponding to higher mass species were dominant, while an enhancement of the TICS is noted at a local maximum of around 700 eV. The mechanisms of formation of such species have been inferred from quantum chemistry calculations exploring different potential energy surfaces, with the major channel being assigned to double ionization of the target molecule followed by electrostatic attraction yielding $[CO_2{\cdot}O_2]^+$ and CO_4^+ structures, as well as CO_3^+.

ACKNOWLEDGMENTS

The authors acknowledge the generous allocation of computer time at the Centro de Computación Científica at the Universidad Autónoma de Madrid (CCC-UAM). This work was partially supported by MICINN (Spanish Ministry of Science and Innovation) Project Nos. PID2019-104727RB-C21 and PID2022-138470NB-I00 funded by MCIN/AEI/10.13039/501100011033 and the "María de Maeztu" (Grant No. CEX2023-001316-M) Program for Centers of Excellence in RD. This study has been performed within the framework of the 21GRD02 BIOSPHERE project supported by the European Association of National Metrology Institutes (EURAMET).

AUTHOR DECLARATIONS

Conflict of Interest

The authors have no conflicts to disclose.

Author Contributions

C. Guerra: Data curation (equal); Formal analysis (equal); Writing – original draft (equal). **M. Leiferman**: Formal analysis (equal); Investigation (equal); Methodology (equal); Software (equal); Writing – original draft (equal). **A. I. Lozano**: Data curation (equal); Formal analysis (equal). **F. Aguilar-Galindo**: Formal analysis (equal); Methodology (equal); Software (equal). **S. Díaz-Tendero**: Conceptualization (equal); Data curation (equal); Methodology (equal); Software (equal); Supervision (equal); Writing – review & editing (equal). **J. C. Oller**: Data curation (equal); Methodology (equal); Validation (equal). **P. Limão-Vieira**: Data curation (equal); Supervision (equal); Validation (equal); Writing – review & editing (equal). **G. García**: Conceptualization (equal); Project administration (equal); Supervision (equal); Validation (equal); Writing – review & editing (equal).

DATA AVAILABILITY

The data that support the findings of this study are available from the corresponding authors upon reasonable request.

REFERENCES

[1] W. J. Witterman, *The* CO_2 *Laser* (Springer-Verlag, Berlin, 1987).
[2] T. Omi and K. Numano, Laser Ther. **23**, 49 (2014).
[3] W. J. Wiegand and W. L. Nighan, Appl. Phys. Lett. **22**, 583 (1973).
[4] A. W. Ehler, J. Appl. Phys. **46**, 2464 (1975).
[5] X.-C. Wang, T.-H. Zhang, Y. Sun, Z.-C. Wu, and Y. T. Zhang, Phys. Plasmas **29**, 023505 (2022).
[6] J. Stierhof, S. Kühn, M. Winter, P. Micke, R. Steinbrügge, C. Shah, N. Hell, M. Bissinger, M. Hirsch, R. Ballhausen, M. Lang, C. Gräfe, S. Wipf, R. Cumbee, G. L. Betancourt-Martinez, S. Park, J. Niskanen, M. Chung, F. S. Porter, T. Stöhlker, T. Pfeifer, G. V. Brown, S. Bernitt, P. Hansmann, J. Wilms, J. R. Crespo López-Urrutia, and M. A. Leutenegger, Eur. Phys. J. D **76**, 38 (2022).
[7] W. Wang, R. Snoeckx, X. Zhang, M. S. Cha, and A. Bogaerts, J. Phys. Chem. C **122**, 8704 (2018).
[8] E. A. Ainsworth and A. Rogers, Plant, Cell Environ. **30**, 258 (2007).
[9] A. J. Bloom, M. Burger, J. S. R. Asensio, and A. B. Cousins, Science **328**, 899 (2010).
[10] M. F. Cotrufo, P. Ineson, and A. Scott, Global Change Biol. **4**, 43 (1998).
[11] D. Jenkinson, D. Adams, and A. Wild, Nature **351**, 304 (1991).
[12] B. Bolin, J. Canadell, B. Moore III, I. Noble, and W. Steffen, Science **285**, 1849 (1999).
[13] P. M. Dittman, D. Dill, and J. L. Dehmer, Chem. Phys. **78**, 405 (1983).
[14] K. E. McCulloh, J. Chem. Phys. **59**, 4250 (1973).
[15] C. R. Brundle and D. W. Turner, Int. J. Mass Spectrom. Ion Phys. **2**, 195 (1969).
[16] A. I. Lozano, A. García-Abenza, F. Blanco, M. Hasan, D. S. Slaughter, T. Weber, R. P. McEachran, R. D. Whit, M. J. Brunger, P. Limão-Vieira, and G. García, J. Phys. Chem. A **126**, 6032 (2022).
[17] M. S. Huq, Dissertations, Theses, and Masters Projects, William & Mary, Paper No. 1539623749, 1984.
[18] K. M. A. Refaey and J. L. Franklin, Int. J. Mass Spectrom. Ion Phys. **20**, 19 (1976).
[19] M. S. Huq, L. D. Doverspike, R. L. Champion, and V. A. Esaulov, J. Phys. B: At. Mol. Phys. **15**, 951 (1982).
[20] V. N. Tuan, V. Esaulov, and J. P. Gauyacq, J. Phys. B: At. Mol. Phys. **17**, L133 (1984).
[21] V. A. Esaulov, J. P. Grouard, R. I. Hall, M. Landau, J. L. Montmagnon, F. Pichou, and C. Schermann, J. Phys. B: At. Mol. Phys. **17**, 1855 (1984).
[22] J. F. Paulson, J. Chem. Phys. **52**, 963 (1970).
[23] J. L. Moruzzi and A. V. Phelps, J. Chem. Phys. **45**, 4617 (1966).
[24] L. D. Doverspike, B. T. Smith, and R. L. Champion, Phys. Rev. A **22**, 393 (1980).
[25] J. B. Greenwood, A. Chutjian, and S. J. Smith, Astrophys. J. **529**, 605 (2000).
[26] M. Hayyan, M. A. Hashim, and I. M. AlNashef, Chem. Rev. **116**, 3029 (2016).
[27] C. M. C. Andrés, J. M. Pérez de la Lastra, C. Andrés Juan, F. J. Plou, and E. Pérez-Lebeña, Int. J. Mol. Sci. **24**, 1841 (2023).
[28] S. Jia, S. Ge, X. Fan, K. W. Leong, and J. Ruan, Nanomedicine **16**, 759 (2021).
[29] N. Liu and G. Sun, Ind. Eng. Chem. Res. **50**, 5326 (2011).
[30] T. J. Millar, C. Walsh, and T. Field, Chem. Rev. **117**, 1765 (2017).
[31] M. Mendes, C. Guerra, A. I. Lozano, D. Rojo, J. C. Oller, P. Limão-Vieira, and G. García, Phys. Rev. A **99**, 062709 (2019).
[32] C. Guerra, S. Kumar, F. Aguilar-Galindo, S. Díaz-Tendero, A. I. Lozano, M. Mendes, P. Limão-Vieira, and G. García, Sci. Rep. **11**, 23125 (2021).
[33] C. Guerra, A. I. Lozano, M. Mendes, S. Kumar, J. C. Oller, P. Limão-Vieira, and G. García, Plasma Sources Sci. Technol. **31**, 035011 (2022).
[34] C. Guerra, S. Kuhmar, F. Aguilar-Galindo, S. Díaz-Tendero, A. I. Lozano, M. Mendes, J. C. Oller, P. Limão-Vieira, and G. García, Int. J. Mol. Sci. **23**, 1266 (2022).
[35] C. Møller and M. S. Plesset, Phys. Rev. **46**, 618 (1934).
[36] R. A. Kendall, T. H. Dunning, and R. J. Harrison, J. Chem. Phys. **96**, 6796 (1992).
[37] D. A. McQuarrie and J. D. Simon, *Molecular Thermodynamics* (University Science Books, 1999).
[38] J. Čížek, J. Chem. Phys. **45**, 4256 (1966).
[39] M. J. Frisch, G. W. Trucks, H. B. Schlegel, G. E. Scuseria, M. A. Robb, J. R. Cheeseman, G. Scalmani, V. Barone, G. A. Petersson, H. Nakatsuji, X. Li, M. Caricato, A. V. Marenich, J. Bloino, B. G. Janesko, R. Gomperts, B. Mennucci, H. P. Hratchian, J. V. Ortiz, A. F. Izmaylov, J. L. Sonnenberg, D. Williams-Young, F. Ding, F. Lipparini, F. Egidi, J. Goings, B. Peng, A. Petrone, T. Henderson, D. Ranasinghe, V. G. Zakrzewski, J. Gao, N. Rega, G. Zheng, W. Liang, M. Hada, M. Ehara, K. Toyota, R. Fukuda, J. Hasegawa, M. Ishida, T. Nakajima, Y. Honda, O. Kitao, H. Nakai, T. Vreven, K. Throssell, J. A. Montgomery, Jr., J. E. Peralta, F. Ogliaro, M. J. Bearpark, J. J. Heyd, E. N. Brothers, K. N. Kudin, V. N. Staroverov, T. A. Keith, R. Kobayashi, J. Normand, K. Raghavachari, A. P. Rendell, J. C. Burant, S. S. Iyengar, J. Tomasi, M. Cossi, J. M. Millam, M. Klene, C. Adamo, R. Cammi, J. W. Ochterski, R. L. Martin, K. Morokuma, O. Farkas, J. B. Foresman, and D. J. Fox, Gaussian 16 Revision C.01, Gaussian, Inc., Wallingford, CT, 2016.
[40] T. N. Olney, N. M. Cann, G. Cooper, and C. E. Brion, Chem. Phys. **223**, 59 (1997).
[41] A. Lira, A. A. Martínez, A. Escalante, S. Vergara, and G. Hinojosa, Int. J. Mass Spectrom. **469**, 116681 (2021).
[42] A. A. Martínez-Calderón, M. M. Sant'Anna, and G. Hinojosa, Phys. Rev. A **109**, 032806 (2024).